Available online at www.sciencedirect.com
SCIENCE DIRECT®
Talanta 65 (2005) 1110–1119
Talanta
www.elsevier.com/locate/talanta

Investigations of the optical properties of thin, highly absorbing films under attenuated total reflection conditions: Leaky waveguide mode distortions

Aigars Piruska, Imants Zudans, William R. Heineman, Carl J. Seliskar*

Department of Chemistry, University of Cincinnati, P.O. Box 210172, Cincinnati, OH 45221-0172, USA

Received 26 November 2003; received in revised form 23 March 2004; accepted 30 April 2004
Available online 23 November 2004

Abstract

Spectra of thin highly absorbing Nafion films doped with $Ru(bpy)_3^{2+}$ on SF11 glass substrates were studied by internal reflection spectroscopy using a single reflection configuration. For the system under study, two modes of light interaction with the film are available: attenuation due to evanescent wave penetration and light propagation within the absorbing film. Unlike evanescent wave spectroscopy, light propagation within the film causes distortions in the measured spectra due to leaky waveguide propagation modes. Upon light propagation in a film doped with $Ru(bpy)_3^{2+}$ spectral shifts up to 50 nm to longer wavelengths can occur and additional absorbance peaks can appear in the spectra. These film-based distortions depend on the complex refractive index, the thickness of the film and the angle of incidence. These effects become significant for an extinction coefficient above 0.01 and a film thickness above 200 nm. It is shown that spectral distortions can lead to quite complex dynamics in the internal reflection spectra upon analyte preconcentration in the film. $Ru(bpy)_3^{2+}$ partitioning into the Nafion film causes significant refractive index changes that in turn alter leaky waveguide mode conditions in the film and, can even lead to a reduction of measured absorbance despite the increase in the extinction coefficient of the film.

Keywords: Leaky waveguide; ATR; Spectral distortions; Highly absorbing films

1. Introduction

Currently we are developing a new type of spectroelectrochemical sensor [1,2]. The most utilized form of the sensor consists of a multiple internal reflection element coated with a transparent indium tin oxide (ITO) film that is then overcoated with a chemically selective film [2,3] (see Fig. 1). In order to be detected the target analyte must partition into the selective film and undergo an electrochemical transformation that gives an optical signal (absorbance, fluorescence) change. It is obvious that the chemically selective film plays a critical role in sensor performance. The film selectively preconcentrates the target analyte, often to a concentration approaching one molar, and generally this leads to significantly lower detection limits. The electrolysis potential and wavelength offer additional selectivity complementing that of the film providing, in all, three modes of selectivity. We have successfully used such sensors even in a complicated and harsh radiochemical environment [4].

Attenuated total reflection (ATR) spectroscopy is intrinsically a surface technique that essentially probes only the film and excludes interferences (e.g., other chromophores) in the bulk solution that lack affinity for the film. However, the optical spectroscopy of the analyte in the selective film examined by internal reflection is complicated by several factors. First, the attenuation of light at each reflection depends on the intrinsic optical properties of the materials involved and the geometrical factors of the system. Unlike normal incidence transmission spectra of bulk samples with a long path length, internal reflection spectra of thin films are conditioned much more by reflection at the absorbing film interface and

* Corresponding author. Tel.: +1 513 556 9213; fax: +1 513 556 9239.
E-mail address: carl.j.seliskar@uc.edu (C.J. Seliskar).

0039-9140/$ – see front matter © 2004 Elsevier B.V. All rights reserved.
doi:10.1016/j.talanta.2004.04.041

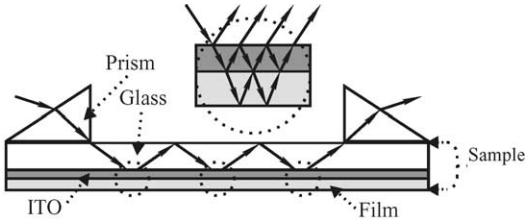

Fig. 1. The principal features of the spectroelectrochemical sensor are shown. The two darkened bottom layers represent indium tin oxide and the chemically selective films. Thickness of these layers is not to scale. Dashed circles indicate several reflections and refractions at each film interface that coherently add (see inset) due to the small thicknesses of the films.

by the interference of light within the film itself. Both of these effects are sensitive to the angle of incidence and the refractive indices of the media. In addition, the interference is sensitive to the thickness of the film(s). Second, the dynamics of the chemical processes in the film (diffusion and electrolysis) produce both optical constant changes and, in most chemically selective films, also significant thickness changes. These film variations can lead to complicated dynamic behavior of measured spectra. Nonetheless, the goal of understanding the details of the physical optics of the spectroelectrochemical sensor, although complicated, is achievable. The optical properties of thin films are well known [5,6] and well established theory can adequately describe them providing the optical constants and thickness of all films are known.

The literature dealing with the chemical spectroscopy of thin films has mainly treated films examined by infrared light. Infrared spectra of thin films by reflectance, transmittance and internal reflectance methods have been discussed by several investigators [7–11]. There are several such reports that are particularly relevant to our work. Hawranek et al. in a series of papers [7–9] discussed sources of errors affecting infrared transmission measurements on neat liquids in thin layer cells. In this case the strong anomalous dispersion of the refractive index of the liquid in a region of strong absorption and the interference of light within the thin layer itself required calculations of the true spectrum of the liquid from experimental measurements. Gunde [10,11] explored theoretically the infrared absorbance band maximum position variation as a function of thin film thickness and compared results with experimental transmission spectra of a silicon dioxide film on a silicon substrate. These results nicely demonstrated a relationship between the absorbance maximum position and the refractive index of the substrate, the oscillator strength of the absorption band, and the thickness of the absorbing film. In general, it was found that only in the limit of infinitely thin film thickness, did the band maximum position coincide with the true vibration frequency. Holm et al. described theory for an attenuation coefficient determination of thin films by ATR spectroscopy in the infrared region. It was shown that measured spectra are complicated by interference of light and are dependent on thickness and refractive index of the film [12].

There are fewer literature reports on thin film induced optical effects on the electronic spectra of films of absorbing materials. Srinivasan and Kuwana [13] studied bulk solution spectra of eosin Y in the presence of a transparent conductive electrode. Spectra measured in the presence of electrode layers exhibited distortions in comparison with attenuated total reflection spectra and show an interference pattern due to the electrode film. Prostak et al. [14] showed that thin (∼5 nm) gold electrodes are suitable for measuring undistorted ATR spectra.

In an effort to improve our understanding of the spectroelectrochemical sensor, we have turned to an examination of a directly related but simpler system as a prototype. In a recent study of such a system we were able to measure, in real time, the detailed optical constants and film thickness changes in Nafion induced by a model analyte ($Ru(bpy)_3^{2+}$) as it partitioned into the film [15]. In this paper we describe the optical waveguide properties of the chemically selective film using that same model system. We are specifically interested in understanding the implications of sensing analytes over broad concentration ranges where such films incorporate analytes with huge preconcentration ratios. In such applications, film concentrations depend on the time used for absorption and the analyte concentration in the sample. As a result, the same film used over time may present low absorbances that require ATR spectroscopy or absorbances that are high and outside of the Lambert–Beer linear region of measurement. It is in this latter concentration regime that we have found severe optical distortions leading to non-linear responses as discussed below. In this paper we present new experimental and theoretical results before, during and after analyte partitioning into a film from solution.

2. Experimental

2.1. Reagents and materials

The following chemicals were used as received: Nafion 5% solution in water and lower alcohols (Aldrich), NaOH (Fisher, analysis grade), tris(2,2′-bipyridyl)ruthenium(II) chloride hexahydrate, (further $Ru(bpy)_3^{2+}$, Aldrich), 3-aminopropyltrimethoxysilane (further APTS, Aldrich). SF11 glass (Schott), SF18 60°–60°–60° prism (Edmund Scientific), index matching fluid (n_D = 1.640, Cargille). The deionized water was obtained using a Barnstead water purification system (18 MΩ). All reagents were used without further purification and all solutions were prepared using deionized water.

2.2. Preparation of Nafion films on SF11 glass

Schott SF11 glass was cut into 1 cm × 4 cm × 2 mm slides and polished (for details see [15]). Polished slides were then washed with methanol, Alconox detergent and extensively rinsed with deionized water and left overnight in aqueous

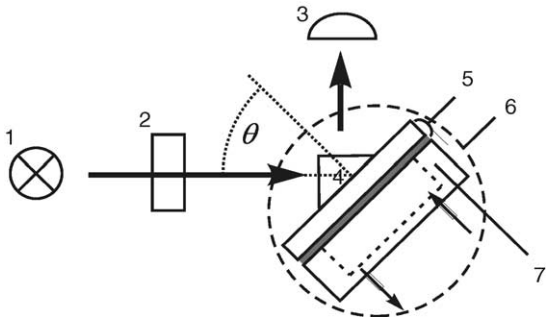

Fig. 2. The experimental arrangement is shown. The diagram numerals are as follows: 1 – lamp; 2 – polarizer and collimating optics; 3 – detector; 4 – SF18 prism; 5 – SF11 slide with film (film depicted with gray layer); 6 – rotation stage; 7 – flow cell.

2 M NaOH solution for surface activation. Activated slides were rinsed with deionized water and placed in 5% APTS solution in acetic acid buffer (pH = 5.5) and kept overnight at 85–90 °C. Nafion solution was spin coated on prepared slides at various spin rates (500, 1000, 6600 rpm) to obtain the desired film thickness.

2.3. Absorbance measurements

The scheme of the experimental setup is depicted in Fig. 2. A Woollam ellipsometer's xenon arc lamp and collimating optics were used as a light source (shown as 1 and 2). A liquid cell (details in [16]), assembled from a base piece (7), a gasket (not shown), a slide (5) and a cover piece (not shown), was placed on a rotation stage (6) and aligned. A SF18 prism (4) was coupled to the slide with index matching fluid (Cargille). Dynamic measurements of $Ru(bpy)_3^{2+}$ uptakes were acquired at 50° and 62° (θ) with respect to the slide normal. Light coming from the prism was filtered with a band pass filter (S143050, Esco Products) to reduce light intensity at wavelengths longer than 500 nm, detected and stored on a computer using an Ocean Optics S2000 spectrometer. To maintain constant concentration of $Ru(bpy)_3^{2+}$ in solution, 500 mL of aqueous 5×10^{-6} M $Ru(bpy)_3^{2+}$ were continuously circulated through the cell at 10 mL min^{-1} using a peristaltic pump (MaterFlex, Cole Palmer Instruments, Co.).

2.4. Measurement of $Ru(bpy)_3^{2+}$ doped film spectra

Nafion films doped with $Ru(bpy)_3^{2+}$ were obtained by soaking films in 1×10^{-4} M $Ru(bpy)_3^{2+}$ overnight. Ellipsometry measurements were done on J. A. Woollam variable angle spectroscopic ellipsometer (vertical setup). Reflectance spectra were obtained in the following way. A SF18 60°–60°–60° (Edmund Scientific) prism coupled with a SF11 glass slide was placed on the ellipsometer's stage and aligned perpendicular to the incoming light beam. Angular scans from 45° to 60° (with respect to the slide normal) were performed. Spectra were obtained for Nafion films and Nafion films doped with $Ru(bpy)_3^{2+}$. Experimental absorbance then was calculated as:

$$A(\lambda) = \log\left(\frac{R_{\text{ref.}}(\lambda)}{R_{\text{doped film}}(\lambda)}\right)$$

where R stands for the experimentally determined reflectance for the reference and doped films.

2.5. Calculations

Experimental data were fitted and theoretical spectra calculated using Woollam WVASE32 software. The computational approach uses the matrix method that describes light propagation through a stack of thin films [5,6]. An optical model was constructed that consisted of a thin film sandwiched between semi-infinite glass and water (or air) layers. The reflectance for any polarization of light and the derived absorbance were calculated using this model. For contour plot analysis a separate algorithm based on the matrix method was written and executed in MathCad 2001. The angle for the absorbance maxima, the magnitude and the phase in the Airy formula were calculated using this algorithm for the spectral interpretation.

In all calculations, manufacturers' material constants for SF11 and SF18 glass and the published constants for water were used [17]. Experimentally determined optical constants for Nafion films previously determined by us were used [15].

3. Theoretical background

For an internal reflection experiment, "absorbance" can be defined similar to that in a normal incidence transmission experiment, namely,

$$A \equiv \log\left(\frac{I_{\text{ref.}}}{I_{\text{sample}}}\right)$$

where $I_{\text{ref.}}$ and I_{sample} are experimentally measured light intensities for a non-absorbing reference film (or prism only) and an absorbing sample, respectively. Since ideally absorbance occurs only by attenuation of the light upon the reflection, the theoretical absorbance of the sample can be calculated as a ratio of reflectances between a reference and the absorbing sample. In a case of a non-absorbing reference sample total reflection is achieved and reflectance is equal to one. A non-zero extinction coefficient in the sample causes attenuation of light and a concomitant decrease of the reflectance. Thus, the expression for absorbance calculation can be simplified and further rewritten as:

$$A = \log\left(\frac{1}{R_{\text{sample}}}\right)$$

where R_{sample} is the reflectance of the absorbing sample.

Despite the equivalent absorbance definition for internal reflection spectroscopy, Lambert–Beer behavior is observable only for small extinction coefficients. The sample ab-

sorbance is directly related to the reflectance, which depends on the optical constants and geometrical factors of the sample (thickness of all films). In general, light interaction with materials at a particular wavelength is described by the complex refractive index, $\tilde{n} = n + ik$. The real part of the complex refractive index (n) is usually called the *refractive index* and it represents the ratio of phase propagation velocity in a vacuum versus that in the given material. The complex part (k), the so-called *extinction coefficient*, describes the attenuation of the light in the material and is the counterpart of the molar extinction coefficient.

At the boundary between two media with different refractive indices, incident light is separated into reflected and transmitted components. The amplitude of reflected components can be found from Fresnel coefficients and is a function of the angle of incidence, the refractive indices of media and the light polarization. Fresnel coefficients for *s* and *p* polarizations are:

$$r_s = \frac{n_1 \cos\theta_1 - n_2 \cos\theta_2}{n_1 \cos\theta_1 + n_2 \cos\theta_2}, \quad \text{and}$$

$$r_p = \frac{n_2 \cos\theta_1 - n_1 \cos\theta_2}{n_2 \cos\theta_1 + n_1 \cos\theta_2}$$

where n denotes the refractive index, θ the angle of incidence, and numerals 1 and 2 indicate values for each medium.

The reflectance from a film or a multilayer stack of films is readily calculated by a coherent summation of all reflected and transmitted components and requires knowing optical constants and thickness of all films [5,6]. For the simplest case of a single film (Fig. 3), reflectance from the film can be calculated using the Airy formula:

$$R_{\text{sample}} = r_{\text{sample}} r^*_{\text{sample}}, \quad r_{\text{sample}} = \frac{r_{01} + r_{12}\ \exp(-i\phi)}{1 + r_{01} r_{12}\ \exp(-i\phi)}$$

where r_{ij} denotes the Fresnel coefficient for the interface between media i and j (0 – high index substrate glass, 1 – absorbing film, 2 – superstrate), * – indicates complex conjugated reflectance coefficient. The quantity ϕ is the phase difference due to light propagation in the film and is calculated as:

$$\phi = \frac{4\pi d}{\lambda} \sqrt{\tilde{n}_1^2 - n_0^2 \sin^2\theta_0}$$

where d is the film thickness and λ the wavelength of light. The Fresnel coefficient and Airy formula are valid for light propagation above and below the critical angle. In the case of an absorbing material, the real refractive index n must be replaced by the corresponding complex refractive index, $\tilde{n}$, and calculations performed using the same expressions.

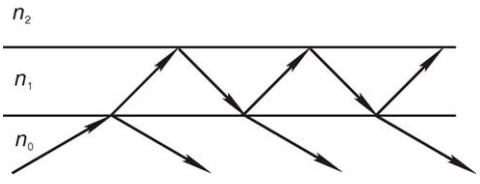

Fig. 3. Definition of a simple optical model undergoing internal reflection at a single absorbing film. The numerals denote: 0 – optical substrate; 1 – film; 2 – superstrate (aqueous liquid medium).

For the system depicted in Fig. 3 two important cases of light propagation in the internal reflection configuration can be identified. In the first case, the refractive index of the film is higher than that of the substrate ($n_1 > n_0 > n_2$). In this case the critical angle can be achieved only at the superstrate and film (1, 2) interface and, upon reflection, light always propagates into the film. In the second case, the refractive index of the film is less than that of a substrate ($n_0 > n_1 > n_2$). Light can propagate into the film if the angle of incidence is less than the critical angle for the film. Above the critical angle with respect to the film, only the evanescent field component of the reflected light penetrates into the film.

The measured absorbance due to evanescent wave interaction with the film is determined by the penetration depth and thickness of the film [18]. The absorbance of a film or a bulk sample at a single wavelength decreases with increasing angle of incidence. For higher angles of incidence, the evanescent wave penetration depth and, thus, the absorbance decreases monotonically with angle.

A different picture is seen for light propagation into the film. The film causes interference of all reflected waves (see Fig. 3) and this greatly affects the magnitude of the absorbance. As opposed to an ATR spectrum of a bulk sample, the angular spectrum of the film at a single wavelength exhibits characteristic maxima and minima [19]. The absorbance maxima increase in magnitude and narrow with increasing angle of incidence. The number of peaks is determined by thickness of the film and its refractive index; their locations in a spectrum are determined by the phase difference of light propagation through the film. The observed absorbance peaks correspond to *leaky propagation modes* in the absorbing film. A planar waveguide, that is, a high index film enclosed between a low index substrate and a superstrate, sustains only discrete propagation modes. The light wave that propagates from one waveguide interface to another and back will exhibit the phase difference:

$$-\phi_{01} + \frac{4\pi\, dn_1 \cos\theta_1}{\lambda} - \phi_{12} = 2\pi m, \quad m = 1, 2, 3, \ldots$$

The introduced phase difference is due to total reflection at interfaces i, j (ϕ_{ij} terms) and propagation of light across the waveguide with thickness d, and θ_1 is the angle of incidence in the waveguide. The phase difference due to total reflection for *s* polarization explicitly is written as:

$$\phi_{1i} = 2 \arctan\left(\frac{\sqrt{n_1^2 \sin^2\theta_1 - n_i^2}}{n_1 \cos\theta_1}\right)$$

In the system considered here, the absorbing film represents a leaky waveguiding structure [20]. As a result, similar phase conditions can be written. The term $-\phi_{01}$ for a leaky waveguide represents the phase difference due to partial reflection and is typically 0 or π. As opposed to true waveguiding, total reflection is achieved only on one side of the guiding

layer, the film/solution interface, and each reflection causes a partial loss of light from the film at the glass/film interface. Light propagation in the film can be achieved at any angle but, similar to planar waveguides, the best propagation conditions in the film are achieved if the phase difference is equal to $2m\pi$, where m is any integer as in the case of true waveguides. The absorbance minima in the angular spectrum are achieved if light has the least propagation distance in the film that occurs for phase difference $(2m + 1)\pi$.

4. Results and discussion

For a proof of concept of our spectroelectrochemical sensor we have used $Ru(bpy)_3^{2+}$ and Nafion as a model analyte and film. Recently, to establish a more detailed understanding of this system, we have studied the dynamics of $Ru(bpy)_3^{2+}$ uptake into Nafion film using spectroscopic ellipsometry [15]. This study quantified the partitioning of $Ru(bpy)_3^{2+}$ into the Nafion film and yielded a description of the extinction coefficient increase of the film and the associated increase of refractive index as the partitioning process occurred. The general shape of the resultant extinction coefficient spectrum for a film with partitioned $Ru(bpy)_3^{2+}$ resembles the normal absorbance spectrum obtained for dilute $Ru(bpy)_3^{2+}$ in aqueous solutions.

4.1. Internal reflection spectra of Nafion films doped with $Ru(bpy)_3^{2+}$

Internal reflection spectra of bulk materials are not conditioned by optical interference and only vary slightly with angle of incidence. In this case, a complete picture can be obtained from a typical spectrum of absorbance as a function of wavelength at any specific angle. On the other hand, the spectra of thin, highly absorbing films, such as those considered here, exhibit a more complicated behavior due to optical interference. In order to demonstrate that, we have chosen to use contour plots (absorbance as a function of angle and wavelength) in our discussion. These contour plots represent a large body of either experimental data or equivalent calculations and we herein refer to them as absorbance-angle-wavelength or, in short, A–θ–λ contours.

A–θ–λ contours of Nafion films of various thicknesses doped with $Ru(bpy)_3^{2+}$ are shown in Fig. 4. In this and in subsequent contour plots the absorbance magnitude is indicated by grayscale. The angle in Fig. 4 and in subsequent plots is the angle of incidence in the top medium (SF18 prism) that was calculated from the experimental angle and the refractive index of the prism. The top panel of three contours represents experimentally measured data; the bottom panel, the theoretically calculated contours for the same films. The optical constants and thickness of the films, necessary for calculations, were separately determined by spectroscopic ellipsometry.

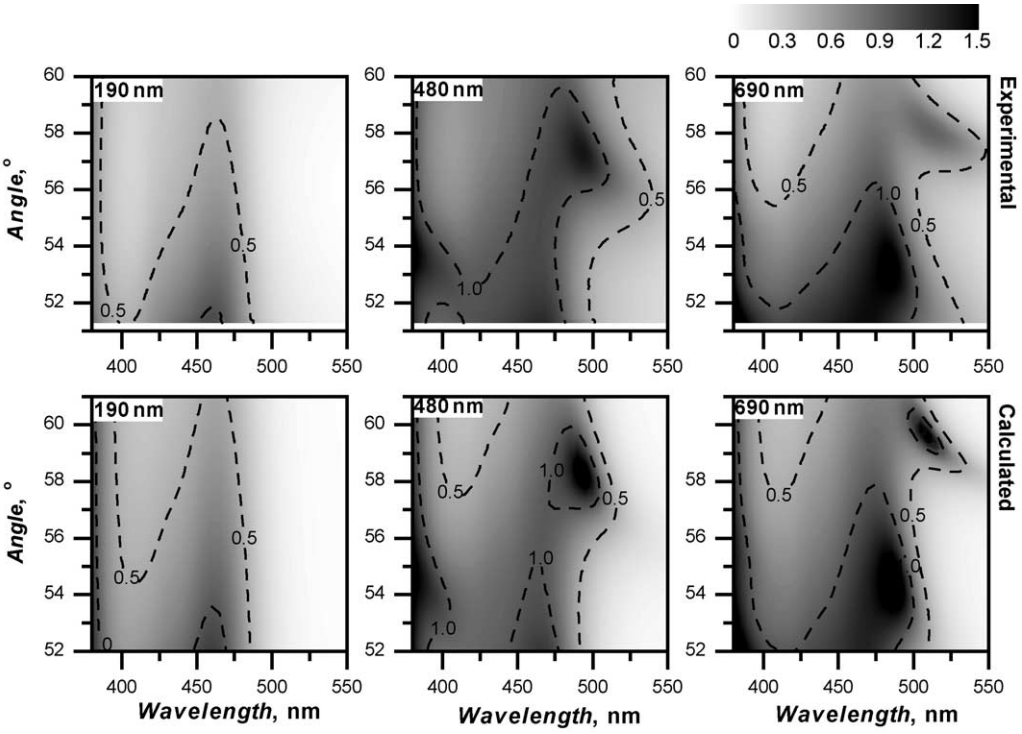

Fig. 4. Experimental (top panels) and theoretical (bottom panels) A–θ–λ contours for three Nafion films of different thickness (190, 480, 690 nm) doped with $Ru(bpy)_3^{2+}$. Absorbance is represented by grayscale and is simultaneously a function of wavelength and angle. The dotted contour lines connect iso-absorbing regions.

The polarizations (*s* and *p*) were averaged for the calculated contours to compare directly with experiment using unpolarized light. The experimentally chosen angular range covers the interval between the critical angle with respect to water and the critical angle with respect to the film. This is just the angular range that can be used to obtain internal reflection spectra for a film in contact with an aqueous medium.

The results in Fig. 4 clearly illustrate the significant influence of the angle of incidence and the film thickness on the absorbance spectra (absorbance spectra correspond to horizontal sections in each plot). Only the thinnest film spectra (190 nm) unambiguously resemble the bulk sample $Ru(bpy)_3^{2+}$ spectrum. The determined minimum in transmittance spectrum obtained for aqueous $Ru(bpy)_3^{2+}$ and, therefore, the maximum extinction coefficient, determined by spectroscopic ellipsometry is about 455 nm wavelength [15]. The absorbance maximum in the thinnest film (190 nm) spectrum is slightly shifted to longer wavelength (maximum at ~462 nm). No other large distortions are observed for this film and the absorbance decreases moving to higher angles of incidence.

The A–θ–λ contours of the two thicker films (480 and 690 nm) also exhibit high absorbance around wavelengths 460 and 470 nm, but new features are also found in the spectra. For both films high absorbance spectral features are found at longer wavelengths and in a relatively narrow angular range. The centers of these maxima lie at 57° and 490 nm, and 58° and 510 nm for the 480 and 690 nm films, respectively. The bottom panel of Fig. 4 contains the equivalent calculated contours. Overall, the agreement between experimental and calculated spectra is seen to be quite good. Looking more critically at this comparison, it can be seen that there is a somewhat different absorbance magnitude for calculated and experimental spectra, and this is especially pronounced in highly absorbing regions farther away from the extinction coefficient maxima. This discrepancy can be attributed to difficulties encountered in acquiring the reference sample spectra as well as film non-uniformity (*vide infra*). The optical constants of all films were determined by spectroscopic ellipsometry that mainly is sensitive to the real part of the refractive index. The imaginary part of the refractive index was found using Kramers–Kronig consistent models [21] and, thus, the accuracy of the extinction coefficient strongly depends on the accuracy of the chosen model.

Analogous absorbance features (highly absorbing regions and peaks tailing to longer wavelength) in calculated contours appear systematically shifted to higher angles of incidence by approximately a degree. This slight offset in angle could be caused by a variety of things including a deviation in the prism angles relative to those specified by the manufacturer, or an angle offset introduced in the alignment procedure.

In order to understand the principal features in the internal reflection spectra and associated A–θ–λ contours of a single absorbing film like $Ru(bpy)_3^{2+}$ doped Nafion, a simple theoretical model with one absorbing film was constructed. In its main features this model closely resembles the experimentally studied system and, in turn, nicely illustrates some of the important aspects of thin film internal reflection spectra. For calculations, no dispersion of the refractive index was assumed for air ($n_2 = 1.00$) and glass ($n_0 = 1.80$). That assumption serves to clearly isolate the importance of the complex refractive index of the absorbing film itself. Optical constants of the model film were calculated using a simple Lorentz oscillator model [22]:

$$n + ik = \sqrt{\varepsilon_\infty + \sum_j \frac{A_j}{E_j^2 - (h\nu)^2 - ih\nu B_j}}$$

where ε_∞ is the high frequency limit dielectric constant, A_j the amplitude of the oscillator, B_j, the width of resonance, E_j, the peak position of the resonance. All parameters A_j, B_j, E_j are given in energy units, namely, eV, and the same obtains for the optical constants. This particular model film contains two Lorentz oscillators, that together exhibit an absorbance band qualitatively similar to that experimentally measured for the doped Nafion film. The values for parameters used were $\varepsilon_\infty = 1.85$, for oscillator 1 – 0.16, 2.75, 0.2 eV (A_j, B_j, E_j) and for oscillator 2 – 10, 6, 0.0001 eV, respectively. The comparison of the experimental optical constants of the doped Nafion film and the Lorentz model film used for calculations is shown in Fig. 5. The principal features of both the strong absorbance at 450 nm indicated by *k* and the associated anomalous dispersion of *n* are well represented by this simple model.

The calculated A–θ–λ contour for the model system is shown in Fig. 6. The calculated contour represents absorbance only for *s* polarization. The choice of one polarization allows one to clearly identify interference maxima in the calculated contour and relate the maxima to the phase differences for light propagation within the film. A very similar result is obtained for *p* polarization with only slightly different interference maxima locations. The contour for randomly polarized light is the superposition of the two *s* and *p* polarization contours. Thus, the maxima in a contour for random polarization are just determined by the numerical values of reflectance for *s* and *p* polarizations.

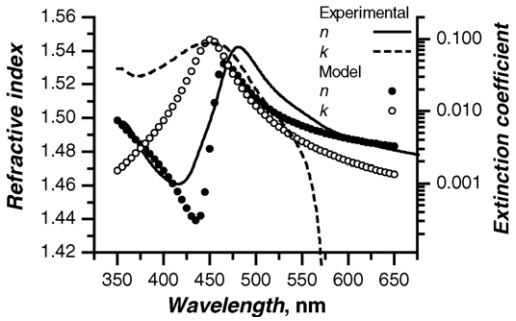

Fig. 5. Comparison of optical constants of a Nafion film doped with $Ru(bpy)_3^{2+}$ and a Lorentz model film used for illustrative calculations. For Nafion film, the ellipsometrically determined refractive index and extinction coefficient are shown. Optical constants for the Lorentz model film were calculated using a two oscillator model as described in the text.

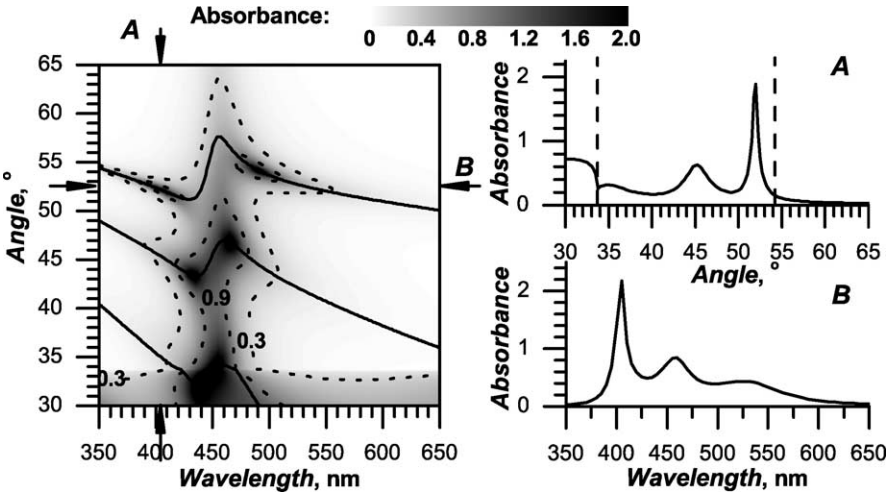

Fig. 6. The A–θ–λ contour (s polarization only, see text) calculated for the model film is shown. Doted lines within the contour connect iso-absorbance regions with magnitudes 0.3 and 0.9. On the right are shown angular (section A) and wavelength (section B) profiles through the contour at the wavelength 410 nm and the angle 52.5°, respectively. The dashed vertical lines in plot A denote the limiting critical angles (see text).

Contour arrow pairs A and B identify cross-sections taken of data for insets to the right that clarify the main features of the absorbance versus wavelength and angle. Inset A shows absorbance as a function of angle at a fixed wavelength of 410 nm. Three distinct absorbance maxima at 52°, 45° and 35° are observed above the critical angle (∼33.8°) with respect to the air/film interface. These maxima correspond to the first three orders of the interference maxima where the phase difference for light propagation in the film constitutes $2m\pi$ with m values 1, 2 and 3, respectively. The solid black lines on the contour itself indicate positions of these interference maxima over the whole contour. Second inset B shows the calculated spectrum at a single angle, 52.5°, that exhibits three distinct absorbance bands. The shape of the angular spectrum (inset A, Fig. 6) is characteristic for a single absorbing film. Since $n_0 > n_1 > n_2$, there are two critical angles, one with respect to the film/air (33.8°) and to the film/glass (54.3°) interface, the distorted part of the spectrum lies in a range between these two critical angles. Above the critical angle with respect to the film, a typical non-distorted internal reflection angular spectrum is seen. Below the critical angle the spectrum is distorted by interference exhibiting several maxima and minima. The number of these features is determined by the complex refractive index, the wavelength and the thickness of the film. Lower order maxima, appearing at higher angles of incidence, are greater in amplitude and narrower in angle than lower ones. In the calculated contour, the interference maxima are present across the whole of the wavelength range. Their positions systematically vary in a way that resembles the shape of the anomalous dispersion of the real part of the refractive index, n.

The regions of highest absorbance in the contour are located on a vertical axis at wavelength about 450 nm that corresponds to the extinction coefficient maximum. Unlike the internal reflection spectrum of a bulk medium, additional absorbance maxima are present in the contour. These maxima are all located on interference maxima (that is, on the solid dark lines) and create high absorbance "islands" similar to ones observed in the experimental contours (see Fig. 4). For lower order interference maxima these highly absorbing regions are located farther away from the axis of the extinction coefficient maximum. The location of highly absorbing regions in the A–θ–λ contours is determined by two factors. First, the phase conditions for leaky waveguiding modes ($2m\pi$) are satisfied; second, the amplitudes of reflected wave at the film surface and the wave that leaks out of the film are important.

Fig. 7 is a combined plot that shows the absorbance spectrum of the first interference maxima that are indicated with top black line in the contour plot shown in Fig. 6. Along with calculated absorbance spectrum in this plot the magnitudes of the two components in Airy formula (r_{01} and $r_{12}\exp(-i\phi)$) are also shown. For an absorbing film, these two parameters are complex numbers and at the interference maxima the

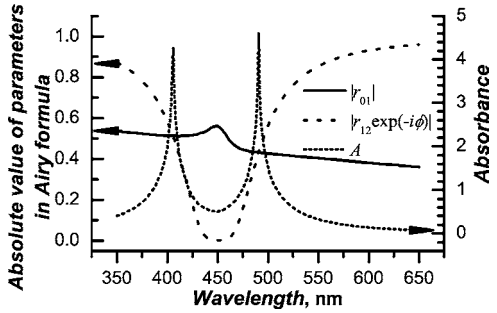

Fig. 7. The absorbance spectrum of the first interference maximum and the magnitudes of the components of the Airy formula are shown. Absorbance and magnitude of Airy formula components for each wavelength were calculated at an angle where the phase difference between r_{01} and $r_{12}\exp(-i\phi)$ equals to π.

phase difference between them is $m\pi$, where m is 1, 3, 5, etc. In turn, the term $r_{01} + r_{12}\exp(-i\phi)$ and, consequently, the reflectance, reaches a minimum. As can be seen from Fig. 7, highly absorbing regions in the A–θ–λ contour occur when two these parameters are of equal magnitude. In turn, that causes the almost complete absorption of light by the film.

From the discussion of the simple Lorentz model above, a few things can be concluded with respect to the experimental $Ru(bpy)_3^{2+}$ doped Nafion film contours. Since leaky mode absorbance maxima are a result of light interference in the film, any non-idealities in the sample film, such as surface roughness and internal non-uniformity of film, would alter the magnitude of absorbance maxima. For example, from the experimental contours in Fig. 4, it can be seen that the 690 nm thickness film exhibits less pronounced leaky mode maxima than the 480 nm film. Thicker films are obtained by spin-coating Nafion solution at lower rates which, in turn, leads to a higher thickness non-uniformity in any thick film and, consequently, to lower absorbance values than one might calculate.

Two additional problems are involved in the experimental procedure. High absorbance requires measurement of low light intensities and that leads to higher uncertainties in the acquired data in regions of high absorbance. On the other hand, for absorbance calculations, the baseline spectrum has to be determined. The determination of the baseline is not always straightforward. The baseline could be measured for a different film sample or acquired just as the light source spectrum itself and leading to two possible definitions of the baseline. Both of these choices introduce an ambiguity whose underpinnings condition the absolute magnitudes contained in acquired experimental spectra, especially in highly absorbing spectral regions.

4.2. $Ru(bpy)_3^{2+}$ diffusion in Nafion

The optical effects discussed so far have described static systems. The situation for dynamic systems is more complicated. The conditions for interference in the film depend on the complex refractive index and the thickness of the film. Dynamic changes of optical constants and the film thickness thus cause associated changes in the interference patterns or leaky waveguiding in the film. To show the influence of leaky waveguiding modes on internal reflection spectra a set of Nafion films with various thicknesses were prepared and the partitioning of $Ru(bpy)_3^{2+}$ into them was monitored by internal reflection spectroscopy in the visible region. The spectra were measured at two different angles. One set of experiments was performed at 62°, allowing only penetration of the evanescent wave into the film; another set was acquired at 50°, which allowed light propagation in the film. The Cauchy dispersion of the prism and the slide refractive index causes a slight variation of the actual angle of incidence of light falling on the film. The experimental conditions at 62° correspond to an angle range from 61.1° (at 380 nm) to 61.2° (at 650 nm); but for 50°, from 54.4° to 54.2°, respectively.

Experimental absorbance–wavelength–time contours for $Ru(bpy)_3^{2+}$ partitioning into Nafion films of various thickness are shown in Fig. 8. In these contours, a vertical slice through the contour gives the absorbance spectrum at the chosen time. The top panel represents data acquired at 50°, the lower at 62°. Several striking differences are apparent. First, data acquired at the higher angle of incidence exhibit essentially non-distorted spectra, although considerably less in absorbance magnitude than data acquired at lower angle of incidence. At 62°, the magnitude of the absorbance and the spectral shape is not appreciably affected by film thickness. No absorbance maxima other than the one that coincides with the maximum of the $Ru(bpy)_3^{2+}$ extinction coefficient are observable.

$Ru(bpy)_3^{2+}$ partitioning into Nafion observed at the lower angle of incidence exhibits a more complicated behavior. Only for the thinnest film (163 nm thickness) is the spectrum in time similar to an ATR spectrum with only the evanescent wave penetrating into the film. Spectra for thicker films (395 and 573 nm thicknesses) show considerable distortions, a significant red shift of the absorbance maxima, and a new absorbance maximum is observed. For the 395 nm thick Nafion film a new maximum appears during partitioning, then shifts to 490 nm, and subsequently disappears. Similarly, the 593 nm thick film shows an additional maximum that increases in magnitude and shifts to 492 nm persisting until film saturation.

The dynamics of the ATR spectra of the thinner films (163 and 395 nm) match reasonably well with calculations. Calculations predict no distortions for the thinnest film, and the appearing and subsequent disappearing of an absorbance peak at 490 nm during $Ru(bpy)_3^{2+}$ partitioning. Experimentally, the thickest film shows a gradual increase of absorbance and simultaneous shift of the absorbance maximum to 490 nm. The associated calculations, however, also suggest an appearing and disappearing peak due to the first order leaky waveguide mode as well as the subsequent appearing of another peak due to the second order leaky mode at 490 nm. However, no peak that would correspond to the first order leaky mode was observed during the partitioning. In previously shown contours the first order absorbance maxima were considerably less in magnitude than the second order maxima, especially for the larger film thicknesses. These thicker films are poorer in optical quality due to the slow spin rates that were used to produce them. In turn, poor film quality could disrupt the interference in film and, thus, lower the experimentally observed absorbance. While this is a plausible explanation, we continue our efforts to understand these discrepancies between experimental and theoretical data.

The principal factors that influence the absorbance are the refractive index, the extinction coefficient and the thickness of the film. Our previous studies indicated that an air-equilibrated Nafion film exposed to water underwent fast swelling, up to 37% relative to the initial film thickness. During the partitioning of $Ru(bpy)_3^{2+}$ into a water equilibrated Nafion film, relatively minor changes in film thick-

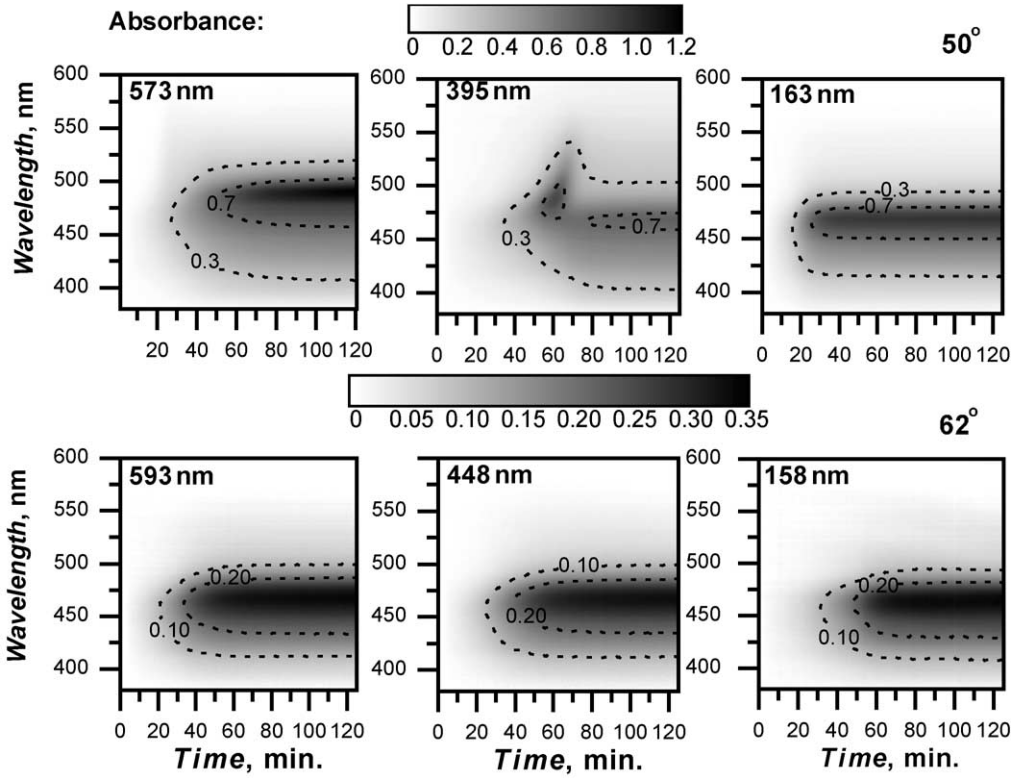

Fig. 8. Dynamics of $Ru(bpy)_3^{2+}$ partitioning into Nafion film observed at a 50° angle (top panels) and at 62° angle (bottom panels) are shown for three different film thicknesses each. An absorbance scale is positioned above each set of panels indicating the range of absorbance measured. The thickness of each film measured before beginning each experiment is indicated in the upper left of each graph. Dashed contour lines connect iso-absorbing regions.

ness occurred [15]. However, the incorporation $Ru(bpy)_3^{2+}$ into the Nafion film causes a considerable increase of the extinction coefficient of the film. Accumulation of $Ru(bpy)_3^{2+}$ in the film also leads to an increase of the film refractive index over the entire visible spectral region. The refractive index and extinction coefficient are interconnected by the Kramers–Kronig relationship [21], and the increase of the extinction coefficient coincides with anomalous dispersion of refractive index across the absorbance band.

The variations of optical constants of the film in time then continuously change the interference effects in the film. At the beginning of the partitioning process, when the film extinction coefficient is relatively small, the absorbance band is close to the extinction coefficient maximum and the peak shape resembles an ATR spectrum of the bulk material. Upon increase of the film extinction coefficient, interference effects within the film can lead to higher absorbance at wavelengths displaced to the side of the extinction coefficient peak. Just this case was illustrated in the calculated contour for the simple Lorentz model shown in Fig. 6. For a single angle absorbance measurement of a thick film, that could initially appear as absorbance band formation close to the true $Ru(bpy)_3^{2+}$ extinction coefficient maximum. Later in time that absorbance maximum shifts to lower or higher wavelength producing a shoulder in the original spectrum. The actual position of the maximum in the spectrum is determined by the phase conditions and the chosen angle of incidence. On the other hand, thin film spectra do not exhibit such leaky waveguide mode distortions due to the small phase difference that is introduced upon light propagation in the film.

5. Conclusions

The studies presented in this paper showed that the absorbance spectra of thin films measured by internal reflection spectroscopy can be severely distorted due to purely optical effects. The absorbance spectrum not only depends on the extinction coefficient, but the refractive index and thickness of film as well. For absorbance measurements two cases can be distinguished – absorbance caused by attenuation of the evanescent field and by the attenuation of light that results from leaky waveguiding in the lossy film. The latter case offers higher sensitivity, but is complicated by the intrinsic optical properties of a film. In an ATR spectrum of a bulk sample, the absorbance maximum is only slightly shifted from the maximum in the molar extinction coefficient, perhaps on the order 10–20 nm in the visible region. Leaky waveguiding in the film, on the other hand, can severely distort the spectrum, especially for a film with an extinction coefficient, *k*, above 0.01. The absorbance maximum can also be considerably shifted from the true maximum in the molar extinction

coefficient of the partitioned chromophore. In addition, several new absorbance maxima can also appear and disappear in time during the partitioning process.

Acknowledgements

This work was supported by a grant awarded by the Environmental Management Science Program of the U.S. Department of Energy, Office of Environmental Management (DE-FG07-99ER62311). The purchase of the Woollam spectroscopic ellipsometer was made possible by a grant from the Hayes Fund of the State of Ohio. Two of us (AP and IZ) were supported by an Ohio Board of Regents Doctoral Investment Award.

References

[1] Y. Shi, A.F. Slaterbeck, C.J. Seliskar, W.R. Heineman, Anal. Chem. 69 (1997) 3679.
[2] Y. Shi, C.J. Seliskar, Chem. Mater 9 (1997) 821.
[3] L. Gao, C.J. Seliskar, Chem. Mater. 10 (1998) 2481.
[4] M.L. Stegemiller, W.R. Heineman, C.J. Seliskar, T.H. Ridgway, S.A. Bryan, T. Hubler, R.L. Sell, Environ. Sci. Technol. 37 (2003) 123.
[5] P. Yeh, Optical Waves in Layered Media, Wiley, New York, 1988.
[6] O.S. Heavens, Optical Properties of Thin Solid Films, Dover Publications Inc., New York, 1991.
[7] J.P. Hawranek, P. Neelakantan, R.P. Young, R.N. Jones, Spectrochim. Acta A 32A (1976) 75.
[8] J.P. Hawranek, P. Neelakantan, R.P. Young, R.N. Jones, Spectrochim. Acta A 32A (1976) 85.
[9] J.P. Hawranek, R.N. Jones, Spectrochim. Acta A 32A (1976) 99.
[10] M.K. Gunde, B. Aleksandrov, Appl. Spectrosc. 44 (1990) 970.
[11] M.K. Gunde, Appl. Spectrosc. 46 (1992) 365.
[12] R.T. Holm, E.D. Palik, Appl. Opt. 17 (1978) 394.
[13] V.S. Srinivasan, T. Kuwana, J. Phys. Chem. 72 (1968) 1144.
[14] A. Prostak, H.B. Mark Jr., W.N. Hansen, J. Phys. Chem. 72 (1968) 2576.
[15] I. Zudans, W.R. Heineman, C.J. Seliskar, J. Phys. Chem. B 108 (2004) 11521.
[16] I. Zudans, C.J. Seliskar, W.R. Heineman, Thin Solid Films 426 (2003) 238.
[17] E.D. Palik, Handbook of Optical Constants of Solids, Academic Press, San Diego, 1998.
[18] N.J. Harrick, Internal Reflection Spectroscopy, Harrick Scientific Corporation, New York, 1987.
[19] M. Leitz, R.P. Podgorsek, H. Franke, J. Woods, Appl. Phys. Lett. 77 (2000) 2674.
[20] R. Ulrich, W. Prettl, Appl. Phys. 1 (1973) 55.
[21] W.J. Tropf, M.E. Thomas, T.J. Harris, in: M. Bass (Ed.), Handbook of Optics, McGraw-Hill, Inc., New York, 1995, pp. 33.01–33.101.
[22] R.A. Paquin, in: M. Bass (Ed.), Handbook of Optics, McGraw-Hill, Inc., New York, 1995, pp. 35.01–35.78.